

ORIGINAL Article

On the Origin of Hemoglobin Cooperativity under Non-equilibrium Conditions

Rosella Scrima¹, Sabino Fugetto¹, Nazzareno Capitanio¹, Domenico L. Gatti^{2,*}

¹ Department of Clinical and Experimental Medicine, University of Foggia, Via L. Pinto 1, Foggia, Italy

² Department of Biochemistry, Microbiology and Immunology, Wayne State University School of Medicine, 540 E. Canfield Avenue, Detroit, MI, USA

*Corresponding authors: Domenico Gatti, Department of Biochemistry, Microbiology and Immunology, Wayne State University School of Medicine, 540 E. Canfield Avenue, Detroit, MI, USA; dgatti@med.wayne.edu

Submitted: March 18, 2022; Revised: May 23, 2022; Accepted: June 01, 2022; Published: June 30, 2022

Citation: Scrima R, Fugetto S, Capitanio N, Gatti DL. On the Origin of Hemoglobin Cooperativity under Non-equilibrium Conditions. *Discoveries* 2022; 10(2): e146. DOI: 10.15190/d.2022.5

ABSTRACT

Abnormal hemoglobins can have major consequences for tissue delivery of oxygen. Correct diagnosis of hemoglobinopathies with altered oxygen affinity requires a determination of hemoglobin oxygen dissociation curve, which relates the hemoglobin oxygen saturation to the partial pressure of oxygen in the blood. Determination of the oxygen dissociation curve of human hemoglobin is typically carried out under conditions in which hemoglobin is in equilibrium with O₂ at each partial pressure. However, in the human body due to the fast transit of red blood cells through tissues hemoglobin oxygen exchanges occur under non-equilibrium conditions. We describe the determination of non-equilibrium oxygen dissociation curve and show that under these conditions the true nature of hemoglobin cooperativity is revealed as emerging solely from the consecutive binding of oxygen to each one of the four subunits of hemoglobin until the entire tetramer is saturated. We call this form of cooperativity the *sequential* cooperativity of hemoglobin and define the simplest model that includes it as the *minimalist* model of hemoglobin. A single instantiation of this model accounts for ~70% of hemoglobin cooperativity under non-equilibrium conditions. The *total* cooperativity of hemoglobin can be viewed

more correctly as the summation of two instantiations of the *minimalist* model (each one corresponding to a tetramer of low and high affinity for O₂, respectively) in equilibrium with each other, as in the Monod-Wyman-Changeux model of hemoglobin. In addition to offering new insights on the nature of hemoglobin reaction with oxygen, the methodology described here for the determination of hemoglobin non-equilibrium oxygen dissociation curve provides a simple, fast, low-cost alternative to complex spectrophotometric methods, which is expected to be particularly valuable in regions where hemoglobinopathies are a significant public health problem, but where highly specialized laboratories capable of determining a traditional oxygen dissociation curve are not easily accessible.

Keywords

Hemoglobin, mitochondria, kinetics, models, cooperativity.

Abbreviations

Haemoglobin (Hb); Oxygen dissociation curve (ODC); Oxygen saturation (S_{O2}); Partial pressure of O₂ (P_{O2}); Partial pressure of CO₂ (P_{CO2}); 1,3 diphosphoglycerate (2,3-DPG); Partial O₂ pressure saturating 50% of Hb (P₅₀); Red blood cells (RBCs); 4-(2-hydroxyethyl)-1-piperazineethanesulfonic acid (Hepes); Triethylene glycol diamine tetraacetic acid (EGTA); Monod-Wyman-

Changeux model (MWC); Association rate constant (k_{on}); Dissociation rate constant (k_{off}); Catalytic constant (k_{cat}); Hb tense state (T); Hb relaxed state (R); Cooperativity gain (c_{gain}); Root mean square (rms); Sum of squared errors (sse); R^2 , R-square.

INTRODUCTION

Hemoglobin (Hb) oxygen dissociation curve (ODC), which relates oxygen saturation (S_{O_2}) and partial pressure of oxygen in the blood (P_{O_2}), is an important tool for understanding how blood carries and releases oxygen¹.

Classically, factors recognized to influence the ODC include the local CO_2 partial pressure (P_{CO_2}), pH, temperature, as well as allosteric metabolites like 2,3 diphosphoglycerate (2,3-DPG). The curve is shifted to the right (i.e. lower saturation for a given P_{O_2}) by higher P_{CO_2} , greater acidity (lower pH), higher temperature, and higher concentration of 2,3-DPG¹⁻⁷. The factors that shift the ODC to the right are directly relevant to the conditions that prevail in metabolizing tissues, as they facilitate the unloading of oxygen from hemoglobin. The converse occurs during passage through the pulmonary capillaries, with the greater affinity accompanying a shift of the ODC to the left aiding the uptake of oxygen⁸.

The partial pressure of oxygen in the blood at which hemoglobin is 50% saturated is known as the P_{50} . The P_{50} of normal hemoglobin is approximately 26 mmHg at a partial CO_2 pressure of 40 mmHg⁷. In the presence of disease or other conditions that change hemoglobin oxygen affinity and, consequently, shift the curve to the right or left, the P_{50} changes accordingly⁹. Low affinity hemoglobins are characterized by higher P_{50} , and high-affinity hemoglobins by a lower P_{50} . Such abnormal hemoglobins can have major consequences for tissue delivery of oxygen, but their effects are mitigated by various compensatory mechanisms, one of which is the hemoglobin concentration. High-affinity molecules, by definition, release oxygen less readily than normal and, because tissue hypoxia is a stimulus to hemoglobin production, affected individuals often have polycythemia; approximately 100 hemoglobin variants with high oxygen affinity have been described in the literature¹⁰. By contrast individuals with low affinity hemoglobins are usually anemic. For example, the abnormal hemoglobin (HbS) of sickle-cell disease (SCD) has reduced oxygen affinity. SCD is a monogenic disorder where the patient is a heterozygous or

homozygous carrier for the β^S allele. This mutation causes a single amino acid substitution from glutamic acid to valine in the β -globin chain of Hb, which results in hydrophobic interactions with adjacent HbS molecules leading to HbS polymers. This polymerization process is triggered at low P_{O_2} and is also dependent on pH. Early recognition in life of the presence of HbS in the blood erythrocytes can better prepare the patient for an SCD 'event' in which rigid, sickled erythrocytes adhere to the endothelium and cause painful vaso-occlusion crises (VOC).

Neonatal cyanosis can also be due to Hb variants with reduced oxygen affinity and a pronounced shift of the ODC to the right. With the introduction of universal screening for congenital heart disease, the finding of abnormal ODC's will likely uncover more neonates with hemoglobinopathies with low oxygen affinity.

Finally, measurement of a complete ODC is important for detecting hemoglobin variants that may escape conventional tests measuring only P_{50} ¹⁰⁻¹². For example, some abnormal ODC's are characterized by bi-phasicism due to the coexistence of both normal and high affinity hemoglobins, and to an exchange of subunits between them^{12,13}. In these cases, measurement of the complete ODC is important to infer the functional properties of the individual hemoglobin components that cannot be easily separated.

Hemoglobin ODC was originally determined by manual methods in which the oxygen saturation of hemoglobin was measured by spectrophotometry at every stepwise change of P_{O_2} by the addition of aliquots of air to the pre-deoxygenated sample in a tonometer, after equilibrium between Hb and O_2 at each P_{O_2} was reached. Although very accurate, this *static* method was very laborious and time consuming. To overcome its limitations, *dynamic* methods were developed in which P_{O_2} was progressively changed in a close vessel, allowing for equilibration in between changes^{1,14-18}. In the most current implementation of these methods, hemoglobin oxygenation and deoxygenation are achieved with highly purified supplies of oxygen and nitrogen or argon gases from cylinders, a Clark oxygen electrode detects the change in oxygen tension, while the resulting increase in oxyhemoglobin fraction is simultaneously monitored by dual-wavelength spectrophotometry at 560 nm and 576 nm¹⁹.

However, equilibrium ODC does not reflect correctly physiological gas exchanges by Hb in the lungs (oxygenation) and in peripheral tissues (deoxygenation) as, due to the fast transit of red blood cells (RBCs) through microcirculation²⁰, hemoglobin O₂ exchanges occur under non-equilibrium conditions. Here, we describe a simple method for the determination of non-equilibrium ODC and analyze the contribution of different components of Hb cooperativity to the curve. Besides mimicking more closely physiological gas exchanges, the methodology offers a low-cost, low-tech alternative to complex and expensive commercial instruments for the determination of equilibrium ODC, which will undoubtedly be valuable in areas of the world where hemoglobinopathies represent a significant public health problem, and highly specialized laboratories capable of determining a traditional ODC are not easily or timely accessible.

MATERIALS AND METHODS

Rat liver mitochondria were purified by differential centrifugation of tissue homogenate as described in²¹, portioned in aliquots of 30-40 mg protein/ml in 0.25 mM sucrose, and stored at -80 °C till used. *Stripped* Hb devoid of allosteric heterotropic factors was prepared from whole human blood of healthy donors²² and its concentration, as HbO₂, was estimated spectrophotometrically from its heme content, with an ϵ_{mM} at 577 nm of 15.4²³. Alternatively, Vacutainer (Becton, Dickinson and company) collected whole blood was used; in this case the HbO₂ concentration was estimated, after dilution of the sample in double distilled water, from the air-equilibrated minus Na₂S₂O₄-supplemented differential spectra, using a $\Delta\epsilon_{mM}$ at 577-568 nm of 4.8 according to²⁴; the Hb content (as heme centers) was typically 9-11 nmol/(ml blood).

Determination of oxygen consumption was carried out by respirometry using Oxygraph-2k (O2k, OROBOROS Instruments, Innsbruck, Austria). The instrument has two measuring chambers (2 ml each) both equipped with a Clark-type electrode; calibration of the instrument was performed according to the manufacturer instructions and all the measurements were carried out at 37 °C. The assay medium constituted by 250 mM sucrose, 1 mg/ml bovine serum albumin, 10 mM KH₂(PO₄), 27 mM KCl, 1 mM MgCl₂, 40 mM

Hepes, 0.5 mM EGTA (pH 7.4) was supplemented with 20-50 µg/ml mitochondrial proteins in the absence or presence of either purified Hb or whole blood samples. Oxygen consumption was initiated by the addition of 10 mM succinate as respiratory substrate in the presence of 2 µM rotenone, an inhibitor of the respiratory chain NADH-ubiquinone oxidoreductase/Complex I. Alternatively, the measurements were carried out with a single-chamber (0.5-1 ml) oxymeter equipped with a Clark type electrode disc (Hansatech Instruments Ltd, King's Lynn, UK).

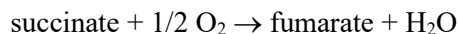
Fitting of the deoxygenation/reoxygenation curves of Hb using four different *kinetic* models (minimalist, Adair, Perutz, MWC) was carried out using in-house code written for Matlab[®] (deposited at https://github.com/dgattiwsu/HB_ODC). Using these models, a single set of rate constants was derived by global analysis of both the deoxygenation and reoxygenation traces.

RESULTS

Non-equilibrium ODC of human hemoglobin. In the following we describe a typical experimental determination of human hemoglobin non-equilibrium ODC.

2 ml of the assay buffer solution (pH 7.4) were placed inside each of the two glass chambers of the Oroboros oxymeter and supplemented with a small amount of purified rat liver mitochondria to a final concentration of 30 µg prot/ml. With the cell open to the environment, the solutions were allowed to equilibrate under stirring with atmospheric O₂ until the observed O₂ concentration (based on an earlier calibration of the electrode²⁵⁻²⁷) remained stable (~183 µM) for a few minutes.

Upon insulating the glass cells from air with glass stoppers (containing a small port for microsyringe additions) progressive reduction of the P_{O₂} in the cell was achieved by adding 10 mM succinate according to the reaction catalyzed by the succinate oxidase segment of the respiratory chain (complexes II+III+IV: succinate dehydrogenase, ubiquinol:cytochrome c reductase, cytochrome c oxidase, respectively):



The final concentration of *cytochrome c oxidase* (the mitochondrial enzyme that uses up O₂ reducing

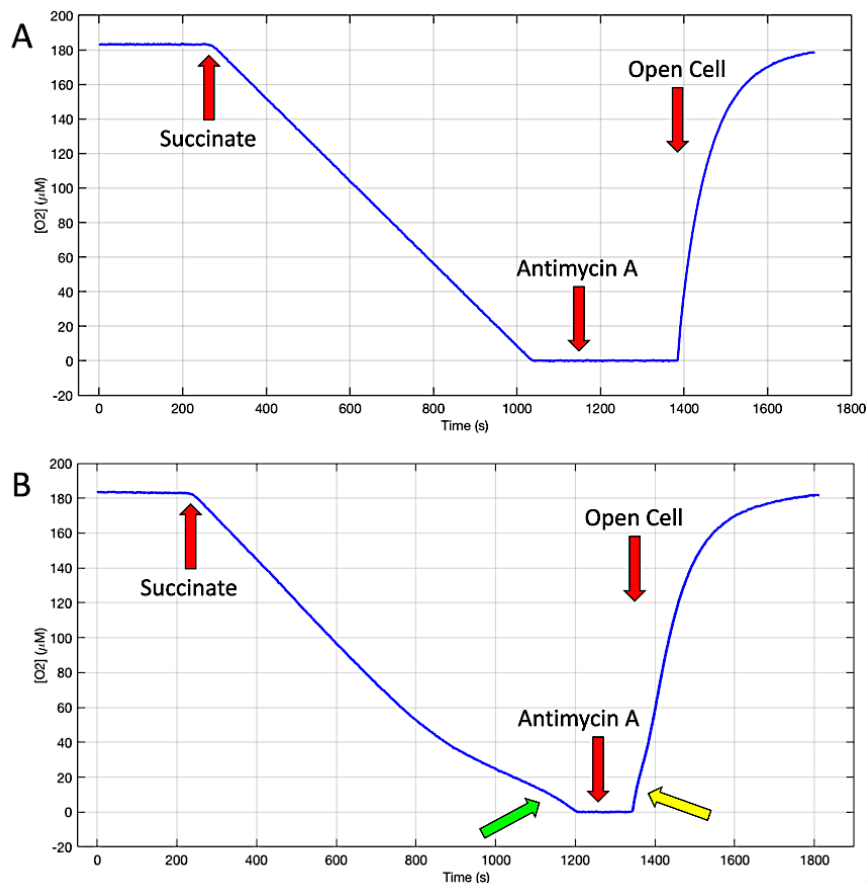


Figure 1. Experimental determination of Hb non-equilibrium ODC

A. Polarographic trace of deoxygenation triggered by succinate, and reoxygenation triggered by reopening the Clark cell in the presence of Antimycin A. **B.** Deoxygenation / reoxygenation cycle in the presence of 50 μM Hb. A green and a yellow arrow point to the deviations from the pattern seen in A.

it to water) in the cell was estimated to be $\sim 0.05 \mu\text{M}$ by visible spectroscopy of the mitochondrial suspension in the 500-650 nanometer range. Upon starting respiration, O₂ concentration decreased linearly until anaerobiosis was reached (**Figure 1A**).

The linear respiratory activity is due to the affinity of cytochrome *c* oxidase for O₂ whose K_M is estimated in the sub-micromolar range^{28,29}. Considering that the instrument limit of detection of O₂ concentration is also in the submicromolar range³⁰, the O₂ concentration is practically never limiting the respiratory flux under the prevailing conditions reported here. After adding 5 μM Antimycin A, an inhibitor of respiration at the level of *ubiquinol:cytochrome c reductase*, the glass stopper was removed, and the cell content was allowed to equilibrate again with air. During this phase oxygen diffuses back in the cell in a non-linear fashion.

When the cycle of deoxygenation/reoxygenation is repeated in the presence of 50 μM (as heme centers) human hemoglobin isolated from blood hydrolysate (**Figure 1B**) the final part of the deoxygenation curve is no longer linear due to the release of oxygen from Hb (green arrow). The initial part of the reoxygenation curve is also slower due to the uptake of oxygen by Hb (yellow arrow).

Since the alterations of the deox-/reoxygenation curves are due to the release/uptake of O₂ by Hb, it is possible to recover the non-equilibrium ODC using a kinetic model of the cell ensemble as a set of reversible reactions involving the species of Hb in different oxygenation state, *cytochrome c oxidase* as the terminal O₂ acceptor, O₂ in the cell, and external air in diffusive equilibrium with the O₂ in the cell, when the latter is open. We have evaluated three different kinetic models (**Figure 2**): **A.** a *sequential* Adair style model with 4 refined parameters (one O₂

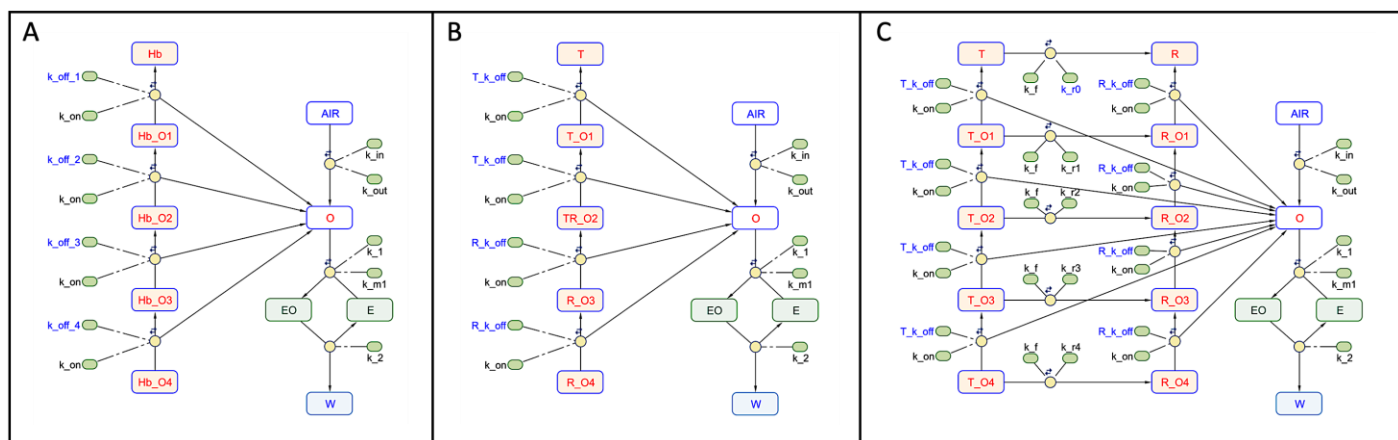


Figure 2. Kinetic models of Hb non-equilibrium ODC

A. Adair model. **B.** Perutz model. **C.** MWC model. Species are shown as rounded rectangles: E = cytochrome *c* oxidase; O = cell O₂; AIR = air O₂; EO = *cytochrome c* oxidase:O₂; W = water. Reactions are shown as yellow circles, rate constants as small, rounded rectangles. Rate constants that are refined in the model are highlighted in blue font. A double arrow over each reaction circle indicates full reversibility. Initial values for all the *on* rate constants were set at 100 μM⁻¹s⁻¹; initial values for the *off* rate constants were set accordingly based on the values of the equilibrium constants for the progressive binding of O₂ to Hb as derived from an initial fit of the oximetric traces with a simple graphic method (Supplementary Information) and using Adair equation^{1,16,33,34}. Initial value for the *k_{cat}* of *cytochrome c* oxidase were derived from the linear phase of respiration supported by succinate. In the Perutz model the species TR_O2 is used to represent the fast conformational transition from T_O2 to R_O2.

k_{off} for each Hb(O₂)_{*n*}, **B.** a *two state sequential* Perutz style model with 2 refined parameters (one O₂ *k_{off}* for Hb(O₂)_{1,2} and one O₂ *k_{off}* for Hb(O₂)_{3,4}), and **C.** a *two state concerted* Monod-Wyman-Changeux (MWC) style model with 3 refined parameters (one *K_{equil}* between a *tense* (T) and a *relaxed* (R) state of Hb, one O₂ *k_{off}* for all T states and one O₂ *k_{off}* for all R states) (reviewed in^{31,32}).

The three models fit equally well the oximetric trace with essentially identical *sum of square errors* (~150 μM²) and *R-square* values (>0.99). Each model provides the contribution of all Hb species (**Figure 3A,D,G**) at all time points (O₂ concentrations). Non-equilibrium ODC's are derived for each P_{O2} value as the ratio between the sum of all the oxygenated species and the total amount of Hb (**Figure 3B,E,H**). The corresponding Hill plots are shown in **Figure 3C,F,I**.

The observed variations in the ODC and Hill plots are due to the fact that for each time point the contributions of individual Hb species are different in the three models. Details of these contributions are shown in a blow-up of the terminal part of Hb deoxygenation phase (**Figure 4A,C,E**), and of the initial part of Hb reoxygenation phase (**Figure**

4B,D,F). Regardless of the model used, concentration peaks are reached in the order Hb(O₂)₄ → Hb(O₂)₃ → Hb(O₂)₂ → Hb(O₂)₁ → Hb during deoxygenation, and Hb → Hb(O₂)₁ → Hb(O₂)₂ → Hb(O₂)₃ → Hb(O₂)₄ during reoxygenation.

In the Perutz and MWC models, intercepts with the X axis of the extrapolated lines from the asymptotic ends of the Hill plot are usually interpreted as the concentration of O₂ at which the concentrations of the unliganded and liganded forms of the T and R states are equal (*K_D*). Better values for these magnitudes are calculated directly from the cross-over points (**Figure 4**) of the T and R forms derived from the kinetic simulations (**Table 1**). Non-linear least-squares fit of Adair equation^{16, 33, 34},

$$S_{O_2} = \frac{K_1[O_2] + 2K_1K_2[O_2]^2 + 3K_1K_2K_3[O_2]^3 + 4K_1K_2K_3K_4[O_2]^4}{4(1 + K_1[O_2] + 2K_1K_2[O_2]^2 + 3K_1K_2K_3[O_2]^3 + 4K_1K_2K_3K_4[O_2]^4)}$$

$$K_1 = \frac{[Hb(O_2)]}{[Hb][O_2]}; K_2 = \frac{[Hb(O_2)_2]}{[Hb(O_2)][O_2]}; K_3 = \frac{[Hb(O_2)_3]}{[Hb(O_2)_2][O_2]}; K_4 = \frac{[Hb(O_2)_4]}{[Hb(O_2)_3][O_2]}$$

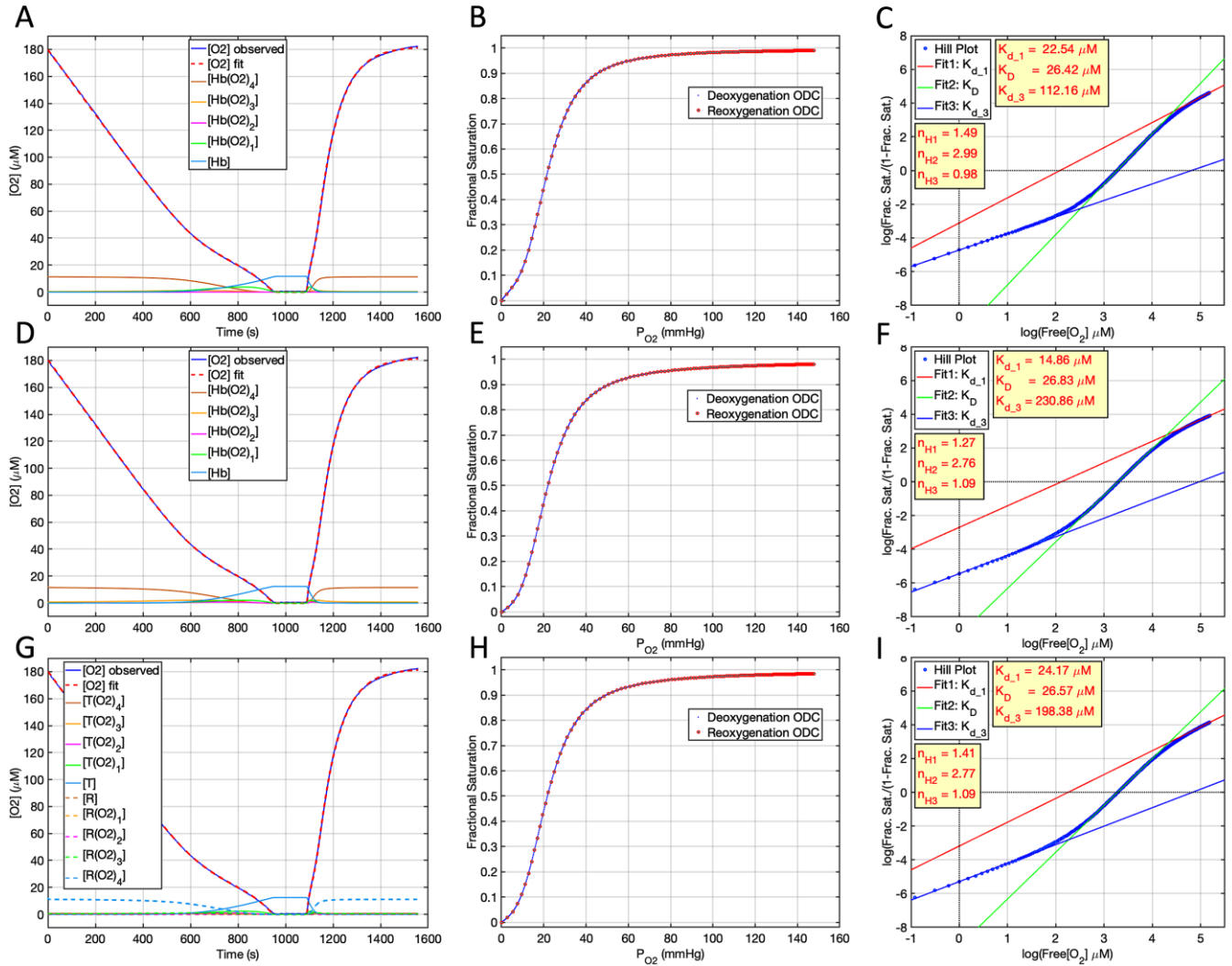


Figure 3. Hb non-equilibrium ODC with the Adair, Perutz, and MWC models

A, D, G. Kinetic fit of the deoxygenation/reoxygenation cycle shown in Figure 1B using the Adair, Perutz, and MWC model, respectively. The refined concentration of Hb tetramers was 11.7, 12.4, 12.5 μM in the Adair, Perutz, and MWC models, respectively. **B, E, H.** ODC's calculated from the fits in **A, D, G**, respectively, using only the deoxygenation (blue dots) or the reoxygenation (cyan circles with red outline) phase. The concentrations of the different Hb species refer to the entire tetramer: therefore, fractional saturation is calculated as $([\text{Hb}(\text{O}_2)_4] \times 4 + [\text{Hb}(\text{O}_2)_3] \times 3 + [\text{Hb}(\text{O}_2)_2] \times 2 + [\text{Hb}(\text{O}_2)]) / ([\text{Hb}_{\text{total}}] \times 4)$. The calculated P_{50} from a non-linear least-squares fit of all the points in the ODC's with Adair equation is ~ 21.9 mmHg. **C, F, I.** Corresponding Hill plots calculated combining points from the deoxygenation and reoxygenation phase.

to the combined experimental points from the deoxygenation and reoxygenation *non-equilibrium* ODC's can be used to derive values for the *equilibrium* Adair constants in the three models (Table 1).

Sources of cooperativity in the models

A common feature of Adair, Perutz, and MWC models is the presence of sequential reactions. A

minimalist model containing four sequential binding reactions, $\text{Hb} \leftrightarrow \text{Hb}(\text{O}_2)_1 \leftrightarrow \text{Hb}(\text{O}_2)_2 \leftrightarrow \text{Hb}(\text{O}_2)_3 \leftrightarrow \text{Hb}(\text{O}_2)_4$, with a single O_2 affinity for all states, and no conformational changes (Figure 5A), fits experimental observations surprisingly well ($\text{sse} = 515.5$, $R^2 = 0.998$) (Figure 5B,C,D), giving origin to a sigmoidal ODC (Figure 5E) and a Hill plot with asymptotic components that suggest the presence of both low and high affinity sites (Figure 5C), despite

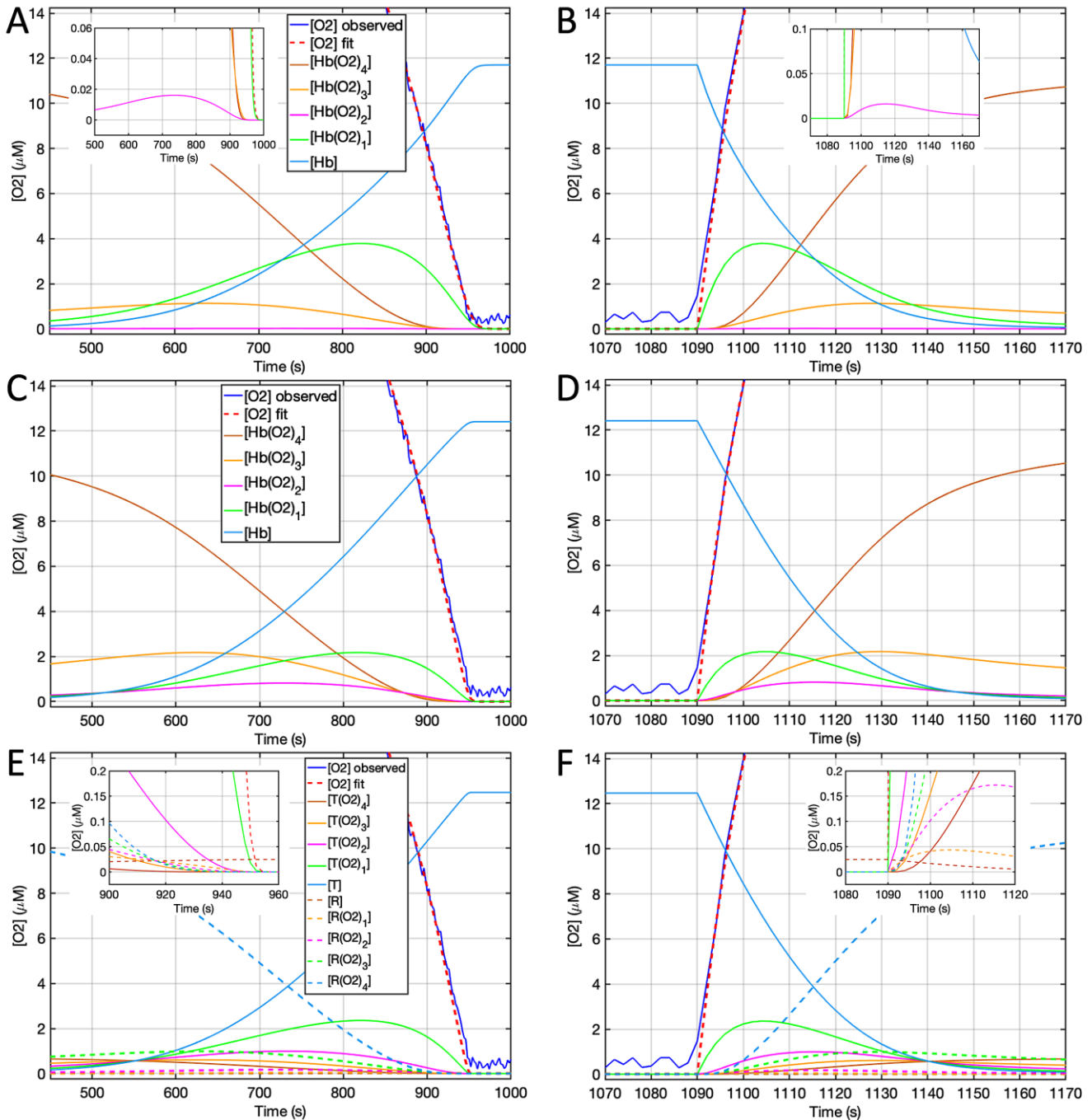


Figure 4. Kinetic fit of the deoxygenation/reoxygenation cycle shown in Figure 1B using the Adair, Perutz, and MWC model, respectively

A,C,E. Blow-up of the terminal part of Hb deoxygenation phase. **B,D,F.** Blow-up of the initial part of Hb reoxygenation phase. Insets in **A,B** show the peaks of $\text{Hb}(\text{O}_2)_2$. Notice the cross-over points at 520 s (**C**) and 1146 s (**D**) between Hb, $\text{Hb}(\text{O}_2)_1$, $\text{Hb}(\text{O}_2)_2$, corresponding to Perutz T conformation, and at 870 s (**C**) and 1098 s (**D**) between $\text{Hb}(\text{O}_2)_2$, $\text{Hb}(\text{O}_2)_3$, and $\text{Hb}(\text{O}_2)_4$, corresponding to Perutz R conformation. Likewise, cross-over points are present at 917 s (**E**, inset) and 1093 s (**F**, inset) between all R states, and at 551 s (**E**) and 1040 s (**F**) between all T states of the MWC model.

none such exist in the model. Accordingly, a fit of Adair equation to the sigmoidal ODC shows that all four Adair constants collapse into a single one

corresponding to the refined k_{on}/k_{off} ratio (**Table 1**). This observation suggests that the most basic source of cooperativity in the Adair, Perutz, and MWC

Table 1. K_D 's (μM) from model refinement, and Adair equilibrium (association) constants (μM^{-1}) for the four steps of Hb oxygenation from a fit of Adair equation to the *non-equilibrium* ODC's

For the Adair and Perutz model, these values are identical to those refined during the optimization of the two models. Notice the collapse of 4 Adair constants into just 2 in the Perutz model, and just 1 in the Minimalist model (see below, Sources of cooperativity in the models). In the MWC model, K_T and K_R are the refined association constants for the T and R states oxygenation, $c = K_T/K_R$, and $L_0 = [T_0]/[R_0]$ is the refined allosteric constant expressing the equilibrium in the absence of any oxygenation between the T and R state of Hb. Allosteric constants L_n for the n different oxygenation levels are not refined, but calculated according to the relationship $L_n = L_0 c^n$.

| | Imai ¹ | Minimalist model | Adair model | Perutz model | MWC model c = 0.1069, $L_0=504.6$, $L_1=53.9$, $L_2= 5.76$, $L_3= 0.62$, $L_4= 0.066$, $K_T = 0.0191$, $K_R = 0.1787$ |
|---------------------|-------------------|--------------------|-------------|--------------------|---|
| $K_{D_crossover}$ | | 27.95 (=1/ K_1) | | | |
| K_{D_Hill} | | 27.73 | 26.42 | 26.83 | 26.57 |
| $K_{DT_crossover}$ | | | | 59.68 (=1/ K_1) | 52.09 (=1/ K_T) |
| $K_{DR_crossover}$ | | | | 12.04 (=1/ K_4) | 5.69 (=1/ K_R) |
| K_1 | 0.0188 | 0.0360 | 0.0368 | 0.0168 | 0.0194 |
| K_2 | 0.0566 | 0.0360 | 0.0002 | 0.0168 | 0.0220 |
| K_3 | 0.4070 | 0.0360 | 2.2237 | 0.0818 | 0.0428 |
| K_4 | 4.2800 | 0.0360 | 0.1730 | 0.0818 | 0.1178 |

models resides in the fact that all three models feature *sequential* binding reaction of O_2 to the four sites of Hb.

We define as the *cooperativity gain* ($cgain$) of a model the *rms* (root mean square) deviation between the model derived ODC and the ODC with the same P_{50} derived from a model containing 4 independent identical O_2 sites. The *cooperative gain* of the minimalist, Perutz and MWC models is shown in **Figure 5E,G,H**.

CONCLUSION

We have presented a typical experiment showing the determination of hemoglobin non-equilibrium ODC, and from it the determination of key parameters such as the P_{50} and the Hill's coefficient. The experimental component of the method requires

minimally the acquisition of a deoxygenation curve of Hb and, optionally, also that of a reoxygenation curve. The computational component is based on the minimization of the *sum of square errors* (*sse*) between an experimentally observed O_2 polarographic trace and a simulated O_2 trace based on a kinetic model of choice (**Figures 2-4**). Since it does not require an optical determination of the Hb saturation, this method can be directly used with a red cell suspension or whole blood without the added complications of the dual-wavelength or full sphere spectrometry that are necessary to eliminate light scattering noise¹⁴. Dedicated instruments capable of carrying out the determination of hemoglobin equilibrium ODC are commercially available at a significant cost, as they require supplies of highly purified gases (i.e., O_2 , N_2 , Ar) from cylinders, a Clark-type electrode to measure

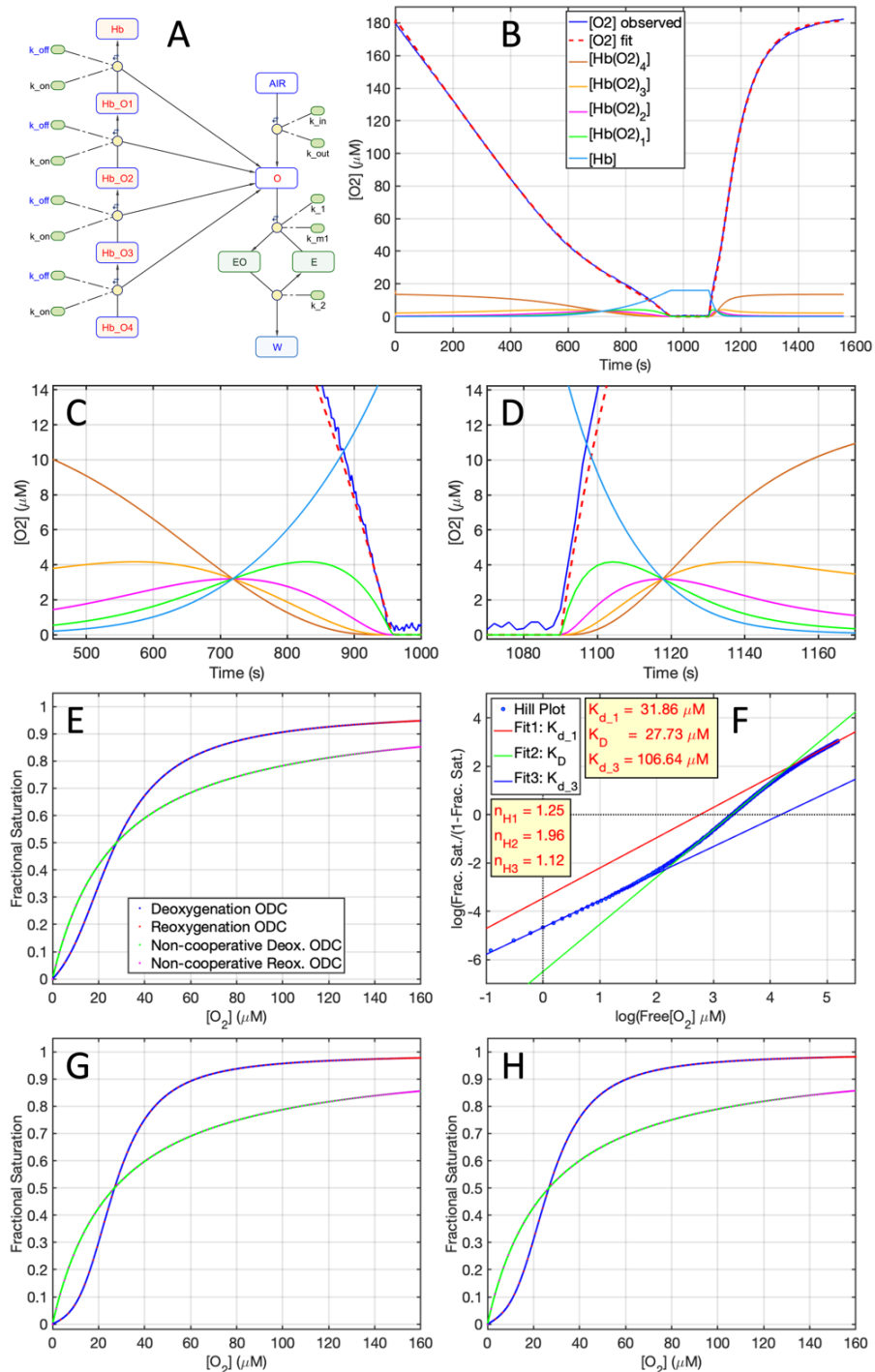


Figure 5. Hb non-equilibrium ODC with the minimalist model

A, Minimalist model with the same O_2 affinity at all binding sites. **B**, Kinetic fit of the deox/reox cycle shown in Figure 1B. **C, D**, Blow-up of the terminal part of Hb deoxygenation phase and the initial part of Hb reoxygenation phase. **E**, ODC calculated from the fit in panel **B**, using only the deoxygenation (blue dots) or the reoxygenation (red circles) phase. The ODC with the same P_{50} derived from a model containing 4 independent identical O_2 sites is shown for the same phases as green and magenta dots ($cgain = 0.1052$). **F**, Corresponding Hill plot calculated combining points from the deoxygenation and reoxygenation phase. **G, H**, ODC's showing the cooperativity gain of the Perutz ($cgain = 0.1505$) and MWC models ($cgain = 0.1526$).

oxygen concentration, and multi-wavelength spectroscopy to detect Hb oxygen saturation inside a

glass cuvette of optical quality. These instruments are typically only accessible in the specialized

hematology laboratories of large medical centers. On the contrary, the protocol described here for the determination of non-equilibrium ODC requires only a widely available glass cell of non-optical quality equipped with a Clark-type electrode, and no flushing of the solutions with purified gases. In our experiment, we have used an in-house preparation of rat liver mitochondria as the source of the respiratory enzymes that drive anaerobiosis. However, a preparation of bacterial membrane particles with comparable properties is commercially available as EC-Oxyrase[®]. Finally, while in our study we have used the proprietary computational platform Matlab[®] for model generation and for the analysis of experimental traces, our code will run also with few modifications in the open-source platform GNU-Octave, and it can be easily converted into fully open source Python code. Thus, altogether, the methodology described here can be easily set up in a small laboratory of a neighborhood clinic as a low-cost, low-tech alternative to the expensive commercial instrumentation available only in large medical centers. A simple determination of Hb ODC can be very useful as part of an initial population screening for hemoglobinopathies before further molecular validation is sought and is expected to be particularly valuable in regions where hemoglobinopathies are a significant public health problem, but highly specialized hematology laboratories are not easily accessible.

It has not escaped our notice that the chemical constants derived from *non-equilibrium* ODC are significantly different from those reported by other authors (i.e.¹, **Table 1**), based on *equilibrium* ODC. This is not surprising, since *non-equilibrium* ODC mimics the physiological condition of red blood cells moving rapidly in the blood stream across regions of different P_{O₂}, while this condition is not reproduced in *equilibrium* ODC.

Three kinetic models (Adair *sequential*, Perutz *two state sequential*, MWC *two state concerted*) were all equally effective in fitting the experimental polarographic traces. Thus, as such, the determination of *non-equilibrium* ODC does not offer any new ways to discriminate between these models. However, the predictions made by the three models with respect to the concentrations of oxygenation and conformational intermediates are quite different (**Figure 4**) and may offer inspiration for future experiments.

The origin of Hb sigmoidal ODC has been a point of intense debate for over a century (reviewed in^{31,32,35}), and this curve is perhaps the most frequently used ‘book perfect’ example of *positive cooperativity*. Our experiments were carried out with *stripped* Hb devoid of allosteric heterotropic factors, and thus under these conditions we observed the intrinsic cooperative behavior of tetrameric Hb. A *minimalist* model, containing no induced (by O₂ binding) or intrinsic conformational equilibria between a *low* and a *high* affinity state, is sufficient to provide, by virtue of the constraint of *sequential* binding reactions of identical affinity, a large fraction (~69% in *cgain* scale) of the cooperative behavior of Hb, as judged by the magnitude of its *cooperative gain* (= 0.1052) with respect to a model containing 4 independent identical O₂ binding sites. We call this basic level of cooperativity observed in the *minimalist* model, the *sequential cooperativity* of Hb. The constraints of sequential binding of oxygen molecules to Hb (rather than, for example, the simultaneous binding of two O₂ molecules to distinct subunits of a single Hb molecule with formation of a single transition state) does not require the invocation of any special structural features of Hb, because according to collision theory the probability of three chemical species reacting simultaneously with each other in a dilute solution in a termolecular elementary reaction is negligible^{36,37}. Therefore, apparent termolecular reactions are typically viewed as non-elementary reactions that can be broken down into a more fundamental set of bimolecular reactions in agreement with the law of mass action.

The *total* cooperativity of Hb under non-equilibrium conditions is accounted for by inclusion in the model of a single conformational equilibrium between a *low* and a *high* affinity state, as shown by the values of the *cooperative gain* in the Perutz (*cgain* = 0.1505) and MWC models (*cgain* = 0.1526). One particularly interesting way of explaining the conceptual relationship between the *sequential* and the *total* cooperativity of hemoglobin is to view *total* cooperativity as the summation of two or more realizations of *sequential* cooperativity. From this point of view, the constraint of sequential reactions is the only true requirement for the emergence of a cooperative behavior. For example, the MWC model (**Figure 2C**) can be viewed as the summation of two *minimalist* models (**Figure 5A**), each one with a different single O₂ affinity for all

states, in equilibrium with each other. In this respect, the Perutz model does not offer any additional insights on the origin of Hb cooperativity, and historically has been perhaps just a source of confusion on this issue.

The observation that Hb cooperativity might originate simply as the consequence of consecutive reactions of a single Hb molecule with four oxygen molecules, paves the way for the exploration of other enzymatic systems, in which phenomena of cooperativity have been attributed solely to conformational changes. At this point it is not clear whether the *sequential* nature of Hb cooperativity was not discovered previously simply because all earlier determinations of Hb ODC were carried out under equilibrium conditions. When a reversible reaction is observed under equilibrium conditions, the forward and backward rates are necessarily identical. However, earlier computational work has revealed that the path followed by the forward and reverse reactions can be different in enzyme conformational space^{38,39}. The constraint of equality between forward and backward rates at equilibrium is more easily fulfilled if two distinct conformations of Hb can affect both rates. Instead, if Hb oxygenation occurs under non-equilibrium conditions, in the absence of a constraint of equality between forward and backward rates at each oxygenation step, hemoglobin may exist almost entirely in one conformational state.

A major contribution of this study to the understanding of the cooperative behavior of allosteric proteins is the indication that the kinetic parameters associated with conformational transitions might be affected by the measuring conditions. The amount of conformational change required to account for the microscopic forward and backward reaction rates of each oxygenation step may depend on the rate at which P_{O2} changes. On this basis, it is tempting to speculate that *in vivo* the relative contribution of the two *minimalist* components that make up the MWC model of Hb, may be modulated by the rate at which erythrocyte move through the capillary bed. In general, one can anticipate that factors that increase this rate (e.g., lower plasma viscosity, higher flexibility of the erythrocytes membrane and cytoskeleton) will magnify the non-equilibrium character of Hb oxygenation, and thus will increase the contribution of only one conformational state of Hb. Conversely, factors that decrease this rate (e.g., higher plasma

viscosity, as it occurs in extreme exercise⁴⁰, infection and/or inflammation⁴¹, or decreased erythrocytes flexibility, as it occurs in an SCD ‘crisis’) will magnify the equilibrium character of Hb oxygenation, and thus will increase the contribution of both conformational states of Hb.

Conflict of Interest

The authors declare no competing interests.

Acknowledgements

This work was supported by a Wayne State University Research Enhancement Program in Computational Biology grant to DLG, and by grants from the University of Foggia to RS, and NC.

Test data and Matlab scripts to carry out a *non-equilibrium* ODC of Hb are freely available at https://github.com/dgattiwsu/HB_ODC.

Authors contributions: Rosella Scrima (rosella.scrima@unifg.it): experimental determination of non-equilibrium ODC; Sabino Fugetto (sabino.fugetto@unifg.it): experimental determination of non-equilibrium ODC; Nazzareno Capitanio (nazzareno.capitanio@unifg.it): study design, manuscript preparation; Domenico L. Gatti (dgatti@med.wayne.edu): Matlab simulations, manuscript preparation; All authors contributed to the writing and/or correction of the manuscript.

REFERENCES

1. Imai K. Adair fitting to oxygen equilibrium curves of hemoglobin. *Methods in enzymology* 1994, 232: 559-576.
2. Bauer C, Schroder E. Carbamino compounds of haemoglobin in human adult and foetal blood. *The Journal of physiology* 1972, 227(2): 457-471.
3. Perrella M, Bresciani D, Rossi-Bernardi L. The binding of CO₂ to human hemoglobin. *J Biol Chem* 1975, 250(14): 5413-5418.
4. Reeves RB. The effect of temperature on the oxygen equilibrium curve of human blood. *Respir Physiol* 1980, 42(3): 317-328.
5. Siggaard-Andersen O. Oxygen-linked hydrogen ion binding of human hemoglobin. Effects of carbon dioxide and 2,3-diphosphoglycerate. I. Studies on erythrolysate. *Scandinavian journal of clinical and laboratory investigation* 1971, 27(4): 351-360.
6. Siggaard-Andersen O, Garby L. The Bohr effect and the Haldane effect. *Scandinavian journal of clinical and laboratory investigation* 1973, 31(1): 1-8.
7. Bock AV, Field H, Jr., Adair GS. The oxygen and carbon dioxide dissociation curves of human blood. *J Biol Chem* 1924, 59: 353-378.

8. Ganong WF. Review of Medical Physiology, 21st edn. McGraw Hill, USA, 2003.
9. Thom CS, Dickson CF, Gell DA, Weiss MJ. Hemoglobin variants: biochemical properties and clinical correlates. *Cold Spring Harb Perspect Med* 2013, 3(3): a011858.
10. Orvain C, Joly P, Pissard S, Badiou S, Badens C, Bonello-Palot N, et al. Diagnostic approach to hemoglobins with high oxygen affinity: experience from France and Belgium and review of the literature. *Ann Biol Clin (Paris)* 2017, 75(1): 39-51.
11. Collins JA, Rudenski A, Gibson J, Howard L, O'Driscoll R. Relating oxygen partial pressure, saturation and content: the haemoglobin-oxygen dissociation curve. *Breathe (Sheff)* 2015, 11(3): 194-201.
12. Imai K, Tientadukul P, Opartkiattikul N, Luenee P, Winichagoon P, Svasti J, et al. Detection of haemoglobin variants and inference of their functional properties using complete oxygen dissociation curve measurements. *Br J Haematol* 2001, 112(2): 483-487.
13. David O, Ivaldi G, Rabino-Massa E, Ricco G. Functional studies on nine different haemoglobins with high oxygen affinity. *Acta Haematol* 2002, 108(3): 132-138.
14. Imai K. Measurement of accurate oxygen equilibrium curves by an automatic oxygenation apparatus. *Methods in enzymology* 1981, 76: 438-449.
15. Imai K. Analysis of ligand binding equilibria. *Methods in enzymology* 1981, 76: 470-486.
16. Adair GS. The hemoglobin system VI: the oxygen dissociation curve of hemoglobin. *J Biol Chem* 1925, 63: 529-545.
17. Severinghaus JW. Blood gas calculator. *Journal of Applied Physiology* 1966, 21(3): 1108-1116.
18. Mohammed Mawjood AH, Imai K. Automatic Measurement of the Red Cell Oxygen Dissociation Curve Identical with the Whole Blood Curve. *The Japanese Journal of Physiology* 1999, 49(4): 379-387.
19. Guarnone R, Centenara E, Barosi G. Performance characteristics of Hemox-Analyzer for assessment of the hemoglobin dissociation curve. *Haematologica* 1995, 80(5): 426-430.
20. Peterson DR, Bronzino JD. *Biomechanics: Principles and Practices*. CRC Boca Raton, FL, 2014, p 7.
21. Frezza C, Cipolat S, Scorrano L. Organelle isolation: functional mitochondria from mouse liver, muscle and cultured fibroblasts. *Nature protocols* 2007, 2(2): 287-295.
22. Hultborn R. A sensitive method for measuring oxygen consumption. *Analytical biochemistry* 1972, 47(2): 442-450.
23. Barzu O. Spectrophotometric assay of oxygen consumption. *Methods in enzymology* 1978, 54: 485-498.
24. Capuano F, Izzo G, Altamura N, Papa S. Spectrophotometric determination with hemoglobin of the rate of oxygen consumption in mitochondria. *FEBS Lett* 1980, 111(1): 249-254.
25. Hitchman ML. *Measurement of Dissolved Oxygen*. Wiley, New York, 1978.
26. Ito S, Yamamoto T. Compensation for measuring error produced by finite response time in determination of rates of oxygen consumption with a Clark-type polarographic electrode. *Analytical biochemistry* 1982, 124(2): 440-445.
27. Li Z. GBH. *Measurement of Mitochondrial Oxygen Consumption Using a Clark Electrode*. *Mitochondrial Disorders* vol. 837. Humana Press, 2012, pp 63-72.
28. Degn H, Wohlrab H. Measurement of steady-state values of respiration rate and oxidation levels of respiratory pigments at low oxygen tensions. A new technique. *Biochim Biophys Acta* 1971, 245(2): 347-355.
29. Bienfait HF, Jacobs JM, Slater EC. Mitochondrial oxygen affinity as a function of redox and phosphate potentials. *Biochim Biophys Acta* 1975, 376(3): 446-457.
30. Gnaiger E. Bioenergetics at low oxygen: dependence of respiration and phosphorylation on oxygen and adenosine diphosphate supply. *Respir Physiol* 2001, 128(3): 277-297.
31. Bellelli A. Hemoglobin and cooperativity: Experiments and theories. *Current protein & peptide science* 2010, 11(1): 2-36.
32. Yonetani T, Kanaori K. How does hemoglobin generate such diverse functionality of physiological relevance? *Biochim Biophys Acta* 2013, 1834(9): 1873-1884.
33. Klotz IM. Hemoglobin-oxygen equilibria: retrospective and phenomenological perspective. *Biophysical chemistry* 2003, 100(1-3): 123-129.
34. Roughton FJ, Adair GS, Barcroft J, Goldschmidt G, Herkel W, Hill RM et al. The thermochemistry of the oxygen-haemoglobin reaction: Comparison of the heat as measured directly on purified haemoglobin with that calculated indirectly by the Van't Hoff Isochore. *Biochem J*. 1936 Nov;30(11):2117-33.
35. Edelstein SJ. Cooperative interactions of hemoglobin. *Annu Rev Biochem* 1975, 44: 209-232.
36. Steinfeld JI, Francisco JS, Hase WL *Chemical Kinetics and Dynamics*. Prentice Hall, 1999.
37. Gillespie DT. A diffusional bimolecular propensity function. *The Journal of chemical physics* 2009, 131(16): 164109-164109.

38. Joseph C, Tseng C-Y, Zocchi G, Tlusty T. Asymmetric Effect of Mechanical Stress on the Forward and Reverse Reaction Catalyzed by an Enzyme. PLOS ONE 2014, 9(7): e101442.
39. Masgrau L, Truhlar DG. The importance of ensemble averaging in enzyme kinetics. Accounts of chemical research 2015, 48(2): 431-438.
40. Nader E, Skinner S, Romana M, Fort R, Lemonne N, Guillot N, et al. Blood Rheology: Key Parameters, Impact on Blood Flow, Role in Sickle Cell Disease and Effects of Exercise. Frontiers in physiology 2019, 10.
41. Sloop GD, De Mast Q, Pop G, Weidman JJ, St Cyr JA. The Role of Blood Viscosity in Infectious Diseases. Cureus 2020, 12(2): e7090.

This article is an Open Access article distributed under the terms of the Creative Commons Attribution License, which permits unrestricted use, distribution, and reproduction in any medium, provided the original work is properly cited and it is not used for commercial purposes; 2022, Scrima R et al., Applied Systems and Discoveries Journals.